Control Induced Explicit Time-Scale Separation to Attain DC Voltage Stability for a VSC-HVDC Terminal

Yijing Chen, Gilney Damm, Abdelkrim Benchaib, Mariana Netto, Françoise Lamnabhi-Lagarrigue

Control Induced Explicit Time-Scale Separation to Attain DC Voltage Stability for a VSC-HVDC Terminal

Yijing Chen * **Gilney Damm** ** **Abdelkrim Benchaib** *** **Mariana Netto** **** **Françoise Lamnabhi-Lagarrigue** *

* *Laboratoire des Signaux et Systèmes (LSS), Supélec, 3 rue Joliot-Curie, 91192 Gif-sur-Yvette, France (e-mail: yijing.chen@lss.supelec.fr, francoise.lamnabhi-lagarrigue@lss.supelec.fr).*
** *Laboratoire IBISC, Université d'Evry-Val d'Essonne, 40 rue du Pelvoux, 91020 Evry, France (e-mail: gilney.damm@ibisc.fr).*
*** *ALSTOM GRID/CNAM, France (e-mail: abdelkrim.benchaib@alstom.com).*
**** *IFSTTAR, 14, Route de la Minire, Bat 824, 78000, Versailles, France (e-mail: mariana.netto@ifsttar.fr).*

Abstract: This paper proposes a novel control scheme to regulate the DC voltage of a VSC terminal. It significantly simplifies the control design process itself and also results in an uncomplicated and efficient control architecture. First, we present an equivalent state-space model established in a synchronous *dq* reference frame. Subsequently, we split the overall system into two interconnected subsystems and suppose that they have different dynamics. Based on this assumption, a reduced model is derived by using singular perturbation techniques. The developed control structure is actually based on this reduced model and an explicit time-scale separation. Simulation results clearly demonstrate that the proposed control strategy can regulate the DC voltage with good performances. Moreover, the real DC voltage can be well approximated by the solution of the reduced model.

Keywords: Control system design; Power systems stability; Singular perturbation

1. INTRODUCTION

Today's electricity industry faces the big challenge of developing more flexible and effective technical solutions for power transmission systems. With the rapid development of power electronics, High Voltage Direct Current (HVDC) systems become more and more interesting compared with traditional High Voltage Alternative Current (HVAC) systems. The main applications of HVDC systems include:

- economical transfer of large amounts of electrical energy over long distances via overhead lines or cables,
- use of underwater power cables with lower electrical losses and smaller costs,
- connection between asynchronous AC grids,
- provision of electrical power to weak AC networks.

HVDC systems are usually divided into two main categories. Early HVDC systems were built up with line-commutated converters (LCC) where each valve is composed of a number of thyristors connected in series. The main drawback of LCC is that the converter has only one degree of freedom, i.e. the firing angle. Thus, the DC current direction is unchangeable. In addition, the converter always consumes reactive power irrespective of the power direction. Furthermore, considerable harmonic distortions may be also produced and then injected to the AC side of the converter. In order to overcome these shortcomings, an attractive alternative for HVDC systems is developed by using voltage-source converters (VSC) (see Flourentzou et al. (2009)) which possess a second degree of freedom. The additional controllability has many advantages, especially the ability to control the reactive power independently of the active power, to improve the harmonic performance and to realize bidirectional power transmission.

This paper is devoted to the control design for a VSC terminal with the application of Pulse Width Modulation (PWM) technology (see Lindberg and Larsson (1996)). Since the VSC terminal possesses two degrees of freedom, there are maximum two possible controllable outputs. Hence, different control configurations exist, for instance, active-reactive power terminal control, DC voltage-AC voltage terminal control and active power-AC voltage terminal control (see Liang et al. (2012)-Chen et al. (2013)).

In the present paper, based on an equivalent averaged state-space model, we design a novel control structure for the VSC terminal in DC voltage-reactive power operation mode. Considering that the system can be divided into

⋆ This work is supported by the French national project WIN-POWER (ANR-10-SEGI-016).

two interconnected subsystems, i.e. a current subsystem and a DC voltage subsystem, the current subsystem could have faster dynamics in contrast with the DC voltage subsystem. Then, a reduced model can be deduced for the DC voltage subsystem, only borne on the slower time scale. Instead of using the original DC voltage subsystem, we develop the control law based on the reduced model. This greatly simplifies the control design process.

The paper is organized as follows. In Section 2, the VSC terminal is modeled in a synchronous dq reference frame. In Section 3, the novel control scheme based on the reduced model is proposed, from which an explicit time-scale separation is derived. The control strategy is validated in Section 4 by numerical simulations. Finally, a summary of the main points is given in Section 5.

2. VSC TERMINAL MODELING

As shown in Fig. 1, a VSC terminal is connected to an AC network via the phase reactor consisting of a large inductance L_l and a small resistance R_l. The phase reactor dominates the dynamic behavior on the AC side of the converter. The DC voltage u_c is provided by the DC capacitor C whose size determines the dynamic behavior on the DC side of the converter. Assuming that the AC network is strong enough, its voltages $v_{l,dq}$ at the point of common coupling (PCC) remain constant regardless of the magnitude and the direction of the active and the reactive power flows. $v_{c,dq}$ are the converter voltages, $i_{l,dq}$ are the currents through the phase reactor and i_c is the DC-bus current representing the power demand/supply from the HVDC grid.

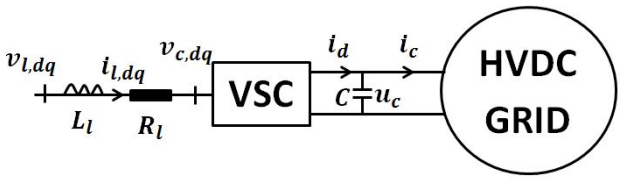

Fig. 1. A simplified configuration of the VSC terminal.

The continuous-time equivalent mathematical model of the VSC terminal introduced in Blasko and Kaura (1997) is expressed:

$$\frac{di_{ld}}{dt} = -\frac{R_l}{L_l} i_{ld} + \omega i_{lq} + \frac{v_{ld}}{L_l} - \frac{u_c}{2L_l} M_d \tag{1}$$

$$\frac{di_{lq}}{dt} = -\frac{R_l}{L_l} i_{lq} - \omega i_{ld} + \frac{v_{lq}}{L_l} - \frac{u_c}{2L_l} M_q \tag{2}$$

$$\frac{du_c}{dt} = -\frac{1}{C} i_c + \frac{3}{4C}(M_d i_{ld} + M_q i_{lq}) \tag{3}$$

where the modulation indices M_{dq} are the control inputs. In practice, M_{dq} are limited to:

$$\sqrt{M_d^2 + M_q^2} \leq 1 \tag{4}$$

The instantaneous active and reactive power flows are given by:

$$P_l = \frac{3}{2}(v_{ld} i_{ld} + v_{lq} i_{lq}); \quad Q_l = \frac{3}{2}(v_{lq} i_{ld} - v_{ld} i_{lq}) \tag{5}$$

For the sake of simplicity, the synchronous dq reference frame is chosen such that the d-axis is fixed to the AC area voltage, i.e. $v_{ld} = V_{l,\text{rms}}$ and $v_{lq} = 0$ and hence the decoupled control on P_l and Q_l can be realized:

$$P_l = \frac{3}{2} v_{ld} i_{ld}; \quad Q_l = -\frac{3}{2} v_{ld} i_{lq} \tag{6}$$

3. CONTROL STRUCTURE

3.1 Control objective

The control objective is to make the DC voltage u_c and the reactive power Q_l track their desired values u_c^* and Q_l^* which are provided by a higher control level. As seen in (6), Q_l is directly regulated by i_{lq}. In order to simplify the problem, we introduce a reference value i_{lq}^* for i_{lq} to satisfy:

$$i_{lq}^* = -\frac{2}{3}\frac{Q_l^*}{v_{ld}} \tag{7}$$

3.2 Control design

In this paper, the control design is inspired by the nonlinear control structure proposed in Lindberg and Larsson (1996). It is mainly based on the following consideration:

> The system (1)-(3) consists of two interconnected subsystems, i.e. the dq current subsystem $S1$ and the DC voltage subsystem $S2$. There exists a control law such that $S1$ has a much faster dynamics than $S2$. Based on the dynamic separation, two subcontrollers are developed to control $S1$ and $S2$, respectively.

Defining $x \triangleq (i_{ld}\ i_{lq})^T$, $z \triangleq u_c$ and $u \triangleq (M_d\ M_q)^T$, the system (1)-(3) can be written in a general form:

$$\dot{x} = f_x(x,\ z) + g_x(x,\ z)\ u \tag{8}$$

$$\dot{z} = f_z(x,\ z) + g_z(x,\ z)\ u \tag{9}$$

with the obvious expressions for $f_x(x,\ z)$, $g_x(x,\ z)$, $f_z(x,\ z)$ and $g_z(x,\ z)$.

The system is a third-order system with two control inputs and hence, only two variables can be controlled directly. Then, the remaining variable may be brought to an equilibrium state via these controllable variables. As seen in (8) and (9), x and u have the same dimension and furthermore, x can be considered collocated with the control input u. An intuitive idea is to develop a control law for u to make x track a reference trajectory x^* yet to be determined. In our case, i_{lq}^* and u_c^* are provided by the higher control level, but there is no ready-made i_{ld}^* for i_{ld}. Consequently, the determination of i_{ld}^* is a crucial step. In this paper, we point out that i_{ld}^* can be derived via a simpler reduced model in two steps:

Current subsystem design Suppose that there exists a state feedback control law $u = h_1(x,\ z)$ such that x in (8) at least locally exponentially converges to x^* as follows:

$$\begin{aligned}\dot{x} &= f_x(x,\ z) + g_x(x,\ z) h_1(x,\ z) \\ &= A\tilde{x} + r(x, x^*)\end{aligned} \tag{10}$$

where $\tilde{x} = x - x^*$ and A is a designed Hurwitz matrix. In control theory, any nonlinear system $\dot{x} = f(x)$ where f is a continuously differentiable map can be divided into a linear part and a nonlinear part. In our case, $r(x, x^*)$ is chosen such that

$$\frac{||r(x, x^*)||}{||\tilde{x}||} \to 0 \text{ as } ||\tilde{x}|| \to 0 \tag{11}$$

The above inequality implies that, for any $\gamma > 0$, there exits a region $\mathbf{B}_r$ such that:

$$||r(x, x^*)|| < \gamma||\tilde{x}|| \tag{12}$$

for all $\tilde{x} \in \mathbf{B}_r$.

The nonlinear part is usually used to improve the performances of the system, for instance, to make the overall system more robust if there exist measurement errors or parameter uncertainties.

The behavior of the nonlinear system is dominated by its linear part in a small neighborhood of the equilibrium point. Consequently, we can impose a fast dynamics on the current subsystem by designing A. Then, $h_1(x,\ z)$ can be obtained by solving (10):

$$h_1(x,\ z) = g_x^{-1}[A\tilde{x} + r(x, x^*) - f_x] \tag{13}$$

under the condition that g_x is nonsingular.

Remark 1. The closed-loop system (10) is exponentially stable at the desired point only when x^* is constant or varying quite slowly compared with x. In this paper, i_{lq}^* is a known constant. Therefore, the remaining task is to design a slowly varying i_{ld}^* whose derivative has negligible effects on the current subsystem.

DC voltage subsystem design Let us suppose that in the current subsystem, x quickly enter its manifold x^* steered by (13). Then, the control input becomes:

$$u_{re} = h_1(x^*,\ z) = -g_x^{-1}(x^*,\ z)f_x(x^*,\ z) \tag{14}$$

By substituting $x = x^*$ and $u = u_{re}$ into (9), we obtain a reduced model:

$$\dot{z} = f_z(x^*,\ z) - g_z(x^*,\ z)g_x^{-1}(x^*,\ z)f_x(x^*,\ z) \tag{15}$$

Denote the solution of (15) as z_{re}. Our goal is to make z_{re} converge to z^*. By recalling the reduced model (15), we can use x^* to control z_{re}. As proceeded in Section 3.2.1, suppose that there exists a state feedback control law:

$$x^* = h_2(z) \tag{16}$$

such that z in (15) can be at least locally asymptotically stabilized at z^*. Then, we have:

$$\dot{z} = f_z(h_2(z), z) - g_z(h_2(z), z)g_x^{-1}(h_2(z), z)f_x(h_2(z), z) \tag{17}$$

$$= A_{re}(z - z^*) + r_{re}(z, z^*) \tag{18}$$

where A_{re} is a designed Hurwitz matrix and $r_{re}(z, z^*)$ represents the nonlinear part satisfying:

$$\frac{||r_{re}(z, z^*)||}{||z - z^*||} \to 0 \text{ as } ||z - z^*|| \to 0 \tag{19}$$

In order to deduce $h_2(z)$ from (17) and (18), we introduce an additional integrator for x^*:

$$\frac{dx^*}{dt} = v_x \tag{20}$$

which yields a higher order reduced model:

$$\frac{dz}{dt} = f_z(x^*,\ z) - g_z(x^*,\ z)g_x^{-1}(x^*,\ z_{re})f_x(x^*,\ z) \tag{21}$$

$$\frac{dx^*}{dt} = v_x \tag{22}$$

By combining (17), (18), (21) and (22), the reference x^* can be finally derived via feedback linearization.

Remark 2. We summarize that the overall control structure for the original system (8)-(9) consists of (13) and (16). The best we can expect is that the solution of the original system z approaches that of the reduced model. The crucial point is to design A and A_{re} which dominate the convergence speeds of x and z in the neighborhood of their respective reference trajectories. By means of singular perturbation techniques, we can prove that if A is designed to make the convergence speed of x much faster, the error between z and z_{re} becomes smaller. Due to the length limitations, a detailed demonstration is not presented here and will be described in a longer paper.

3.3 Application to the VSC terminal

The proposed example is to choose a diagonal matrix for A and $r(x, x^*) = 0$, which means that i_{ld} and i_{lq} can be controlled independently. Then, M_{dq} are deduced:

$$\begin{pmatrix} M_d \\ M_q \end{pmatrix} = -\begin{pmatrix} \frac{2L_l}{u_c} & 0 \\ 0 & \frac{2L_l}{u_c} \end{pmatrix} \cdot \left(\begin{pmatrix} -k_d & 0 \\ 0 & -k_q \end{pmatrix} \begin{pmatrix} i_{ld} - i_{ld}^* \\ i_{lq} - i_{lq}^* \end{pmatrix} - \begin{pmatrix} -\frac{R_l}{L_l} i_{ld} + \omega i_{lq} + \frac{v_{ld}}{L_l} \\ -\frac{R_l}{L_l} i_{lq} - \omega i_{ld} + \frac{v_{lq}}{L_l} \end{pmatrix} \right) \tag{23}$$

with positive k_d and k_q which are used to regulate the convergence speeds of i_{ld} and i_{lq}, respectively. Substitute the resulting expression (23) into (3) and then obtain the reduced model:

$$\dot{u}_c = -\frac{i_c}{C} + \frac{3}{2C}\frac{(-R_l i_{ld}^{*^2} + v_{ld} i_{ld}^*) + (-R_l i_{lq}^{*^2} + v_{lq} i_{lq}^*)}{u_c} \tag{24}$$

where the term $i_{ld}^{*^2}$ explicitly appears. As mentioned before, an additional integrator is introduced:

$$\frac{di_{ld}^*}{dt} = u_d \tag{25}$$

In order to make u_c in (24) converge to u_c^*, several control techniques can be applied. In this work, we use input/output feedback linearization theory. Considering that u_c is the output, its relative degree is two. Consequently, the following Lie derivatives can be deduced:

$$\dot{u}_c = L_{f_0}^1(u_c) \tag{26}$$

$$\ddot{u}_c = L_{f_0}^2(u_c) + L_{g_0} L_{f_0}^1(u_c) u_d \tag{27}$$

where

$$L_{f_0}^1(u_c) = -\frac{i_c}{C} + \frac{3}{2C} \times \frac{(-R_l i_{ld}^{*^2} + v_{ld} i_{ld}^*) + (-R_l i_{lq}^{*^2} + v_{lq} i_{lq}^*)}{u_c} \tag{28}$$

$$L_{f_0}^2(u_c) = -\frac{3L_{f_0}^1(u_c)}{2C}\frac{(-R_l i_{ld}^{*^2} + v_{ld} i_{ld}^* + -R_l i_{lq}^{*^2} + v_{lq} i_{lq}^*)}{u_c^2} \tag{29}$$

$$L_{g_0} L_{f_0}^1(u_c) = \frac{3}{2C}\frac{1}{u_c}(-2R_l i_{ld}^* + v_{ld}) \tag{30}$$

By introducing an auxiliary input θ_d, u_d is obtained:

$$u_d = \frac{1}{L_{g_0} L_{f_0}^1(u_c)}(-L_{f_0}^2(u_c) + \theta_d) \tag{31}$$

where θ_d is designed using linear technique:

$$\theta_d = -c_1(u_c - u_c^*) - c_2 \dot{u}_c \tag{32}$$

Table 1. Parameter values of the VSC terminal.

R_l	L_l	v_{ld}	C	f
0.05 Ω	40 mH	140 kV	20 mF	50 Hz

with positive c_1 and c_2. By substituting (31) and (32) in (24) and (25), the closed-loop system of the reduced model can be written as:

$$\frac{d}{dt}\begin{pmatrix} u_c \\ \dot{u}_c \end{pmatrix} = \begin{pmatrix} 0 & 1 \\ -c_1 & -c_2 \end{pmatrix}\begin{pmatrix} u_c - u_c^* \\ \dot{u}_c \end{pmatrix} \tag{33}$$

where c_1 and c_2 jointly determine the convergence speed of the reduced model. Finally, i_{ld}^* is derived:

$$\frac{di_{ld}^*}{dt} = -\frac{L_{f_0}^2(u_c) + c_1(u_c - u_c^*) + c_2\dot{u}_c}{L_{g_0}L_{f_0}^1(u_c)} \tag{34}$$

As seen in (33), the resulted closed-loop system is a linear second-order system. We can impose a slow dynamics on the reduced model by tuning the values of c_1 and c_2.

Remark 3. In the proposed scenario, the feedback linearization approach is chosen since the properties of linear system can be used to regulate the behavior of the system.

4. SIMULATION RESULTS

In order to evaluate the proposed control method, the VSC terminal is simulated in MATLAB by using the averaged state-space model introduced in Section 2 and then the SimPowerSystems toolbox (see Fig. 5). The system parameters are given in Table 1.

In this paper, several simulation scenarios are considered. All of them initially operate in a steady state with u_c = 300 kV, i_c = 700 A, i_{ld} = 1000 A and i_{lq} = 0 A. In addition, the desired value of i_{lq} is set to zero to get a unitary power factor.

4.1 Performance evaluation using the averaged state-space model

Scenario 1: the choice of the control gains As mentioned in Section 3, the control structure is based on the consideration that the current subsystem has a faster dynamics than the DC voltage subsystem. However, the two dynamics heavily depend on the choice of the control gains. In order to evaluate their effects on the behavior of the system, two cases are simulated where we choose the control gains as $k_{d1} = k_{q1} = 150$ and $k_{d2} = k_{q2} = 50$, respectively. In both cases, we set $c_1 = 225$ and $c_2 = 15$.

The simulation results are displayed in Fig. 2 where the blue and the green lines specify a error band which is a range of ±2% of the final value. As seen in Fig. 2(a), the terminal initially work in the steady condition. At $t = 5$ s, u_c^* increases by 40%, i.e. $u_c^* = 420$ kV (the red curve). Comparing the responses of u_c in Fig. 2(a), we find that u_c in Case 1 has a better performance than in Case 2. On the one hand, the time required for the response of u_c in Case 1 that remains within the error band is about 1.8 s, whereas the time in Case 2 is about 1.9 s. This means that Case 1 has a faster response speed than Case 2. On the other hand, the peak value in Case 1 is also smaller than in Case 2. Figure 2(b) depicts the errors between u_c and $u_{c,re}$ in both cases where a better transient performance is also shown in Case 1. The error in Case 2 is always larger than in Case 1. This phenomenon confirms Remark 2.

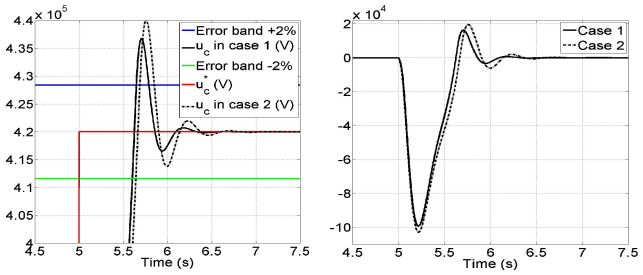

(a) u_c response. (b) Errors between u_c and $u_{c,re}$.

Fig. 2. Performance evaluation of the control gains: $k_{d1} = k_{q1} = 150$ in Case 1 and $k_{d2} = k_{q2} = 50$ in Case 2.

From this scenario, we can say that with the control gains of the DC voltage subcontroller (c_1 and c_2) settled, the performance of the system can be improved by increasing the control gains of the current subcontroller, i.e. k_d and k_q.

In the next scenarios, the control gains are chosen as $k_d = k_q = 2500$, $c_1 = 625$ and $c_2 = 50$.

Scenario 2: Variations in i_c As previously described, the DC-bus current i_c is a measurable variable which represents the power demand/supply from the HVDC grid. Suppose that the power injections from other terminals may be time-varying or may be subjected to some sudden changes. These events drive the HVDC grid into power imbalance and lead to variations in i_c. In this scenario, we verify that the proposed control approach can make the terminal operate as a slack bus to tolerate the variations in i_c.

The sequence of events of i_c applied to the VSC terminal is illustrated in Fig. 3(a) and the responses of related variables are depicted in Figs. 3(b)-3(h).

The responses of u_c and $u_{c,re}$ are shown in Fig. 3(c). The DC voltage always converges to its reference value of 300 kV irrespective of the variations in i_c. We also find that the trajectories of u_c and $u_{c,re}$ are very close to each other. As shown in Fig. 3(f), the discrepancy between the two trajectories is quite small. In this simulation, the error between u_c and $u_{c,re}$ is always less than 20 V as shown in Fig. 3(d). This means that u_c can be closely approximated by the solution of the reduced model. As illustrated in Fig. 3(b), every time i_c varies, i_{ld} and i_{ld}^* react accordingly. From Fig. 3(e), it is obvious to see how close i_{ld} and i_{ld}^* are. The trajectory of i_{ld} almost coincides with its manifold i_{ld}^*. This phenomenon clarifies that i_{ld} quickly approaches its manifold during a short interval. The responses of the control inputs M_{dq} are presented in Figs. 3(g)-3(h). They always satisfy the physical limitation (4). In addition, the response of i_{lq} not presented here always converge to zero.

Scenario 3: Step changes in u_c^* In this scenario, we evaluate the performance of the control strategy when gradually increasing or decreasing the DC voltage reference value by 10%. During the whole simulation, i_c is kept unchanged at 700 A. As illustrated in Fig. 4(a), every two seconds, u_c^* is subjected to a step change (the violet line). Figures 4(c)-

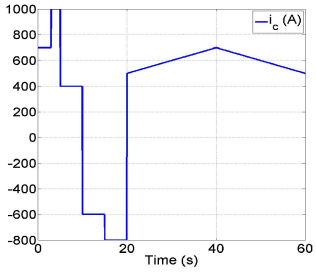

(a) Varying i_c.

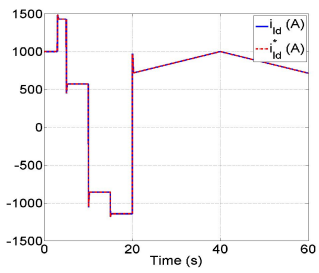

(b) Responses of i_{ld} and i^*_{ld}

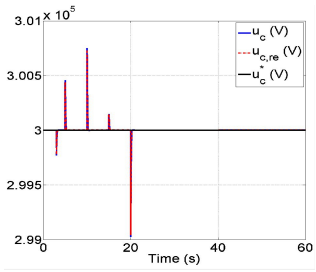

(c) Responses of u_c and $u_{c,re}$

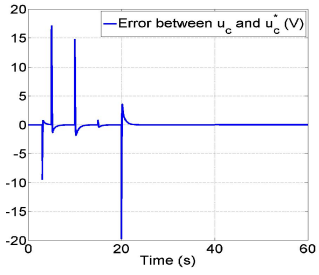

(d) Error between u_c and $u_{c,re}$.

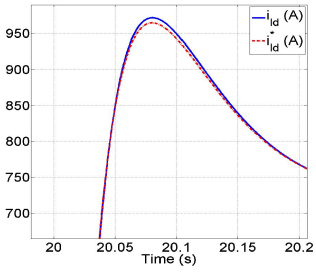

(e) Zoom of i_{ld} and i^*_{ld} around $t = 20.1$ s.

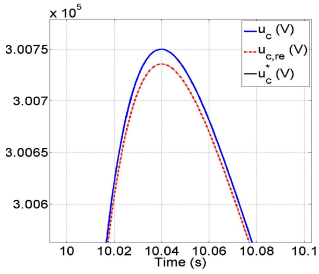

(f) Zoom of u_c and $u_{c,re}$ around $t = 10.04$ s.

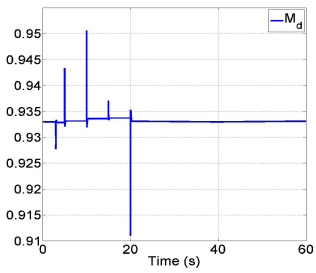

(g) M_d response

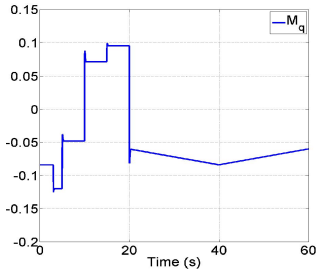

(h) M_q response

Fig. 3. Simulation results corresponding to varying i_c.

4(f) present the zooms of the responses of u_c from which we can get more details. The responses of i_{ld} and i^*_{ld} are illustrated in Fig. 4(b).

After a new reference value $u^*_c = 330$ kV is given at $t = 2$ s, u_c starts to increase as seen in Fig. 4(a). Before $t = 2.1$ s, u_c remains within the error band. In the meantime, i_{ld} attains the corresponding steady state as shown in Fig. 4(b). At $t = 4$ s and $t = 6$ s, the DC voltage reference values are set to 363 kV and 399.3 kV, respectively. It is seen that u_c gives a fast response to follow these new reference values and i_{ld} has a similar performance. Conversely, at $t = 8$ s, u^*_c is required to decrease 10%. With the proposed controller, u_c also decreases until arriving at the new reference value. In this case, we also find that the trajectories of i_{ld} and u_c are very close to the trajectories of i^*_{ld} and $u_{c,re}$, respectively. This phenomenon verifies our

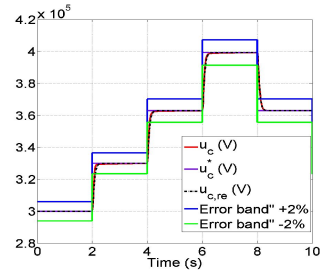

(a) Response of u_c and its reference trajectory u^*_c.

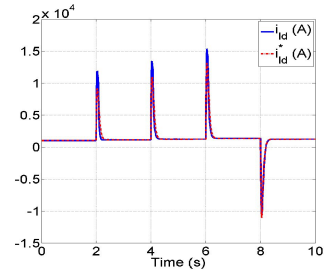

(b) Response of i_d and its manifold i^*_{ld}.

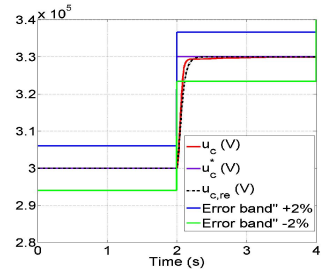

(c) Zoom of u_c and $u_{c,re}$ during $t \in (0, 4)$ s.

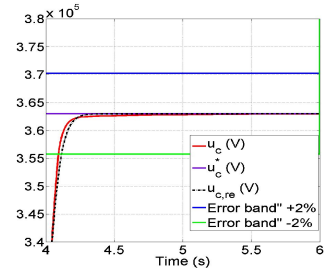

(d) Zoom of u_c and $u_{c,re}$ during $t \in (4, 6)$ s.

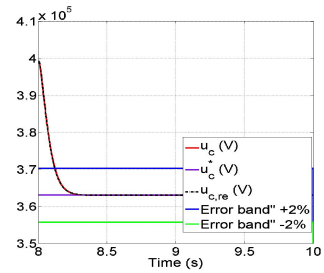

(e) Zoom of u_c and $u_{c,re}$ during $t \in (6, 8)$ s.

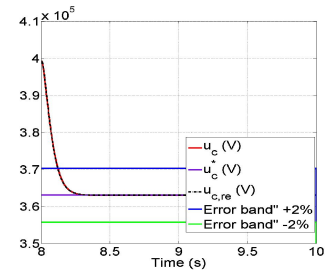

(f) Zoom of u_c and $u_{c,re}$ during $t \in (8, 10)$ s.

Fig. 4. Simulation results with various values of u^*_c.

theoretical analysis. When i_{ld} quickly enters its manifold i^*_{ld} with the current subsystem controller, the behaviors of u_c and $u_{c,re}$ are quite similar.

4.2 Performance evaluation using the SimPowerSystems toolbox

In this section, the developed control scheme is tested with the SimPowerSyesyems toolbox. The base quantities applied in the per-unit system are $V_b = 300$ kV, $S_b = 300$ MVA. The simulated model as shown in Fig. 5 contains three parts:

1. A three-phase source block representing a stiff AC grid and providing the three-phase voltage;
2. The VSC model composed of the phase reactors, the filters, the semiconductor devices, etc;
3. A controlled current source modeling the power demand/supply from the HVDC grid.

The block of the proposed control scheme is implanted into the block of the VSC model. The reference values of u_c and i_{lq} are set to 1 p.u. and 0 p.u., respectively. The system initially operates in a steady state with $u_c = 1$ p.u., $i_c = 0.146$ p.u., $i_{ld} = -0.14$ p.u. and $i_{lq} = 0$ p.u..

The controlled current source generates a DC current i_c as illustrated in Fig. 6. At $t = 2$ s, i_c drops to 0.073 p.u..

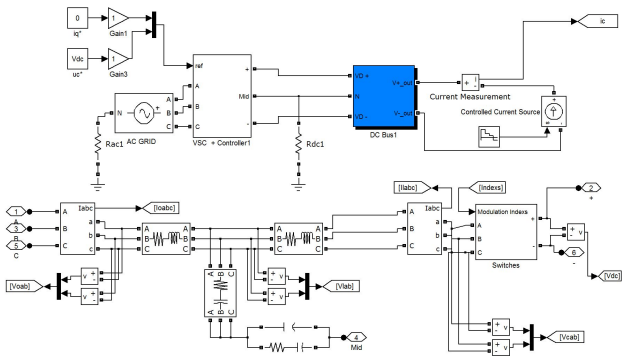

Fig. 5. A configuration of the VSC terminal using SimPowerSystems toolbox.

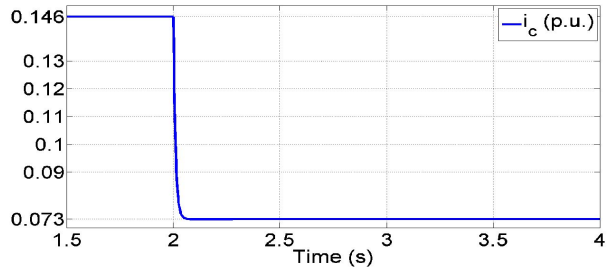

Fig. 6. i_c generated by the controlled current source.

The simulation results are shown in Fig. 7. We see that when i_c suddenly changes, u_c remains around its reference value, i.e. $u_c = 1$ p.u., after a short transient, as shown in 7(a). During this short transient, just some small overshoots exist and they do not threaten the normal operation of the VSC terminal. As shown in Fig. 7(b), i_{lq} is always stabilized around the origin and i_{ld} attains a new steady state which corresponds to the new value of i_c.

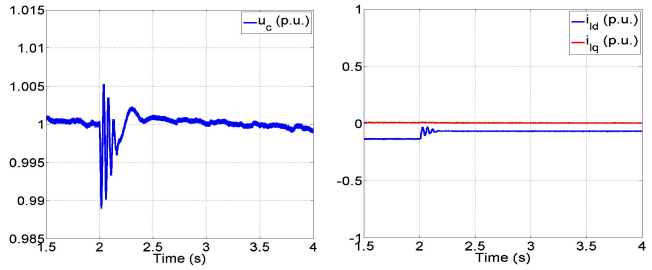

(a) Response of u_c. (b) Response of i_d.

Fig. 7. Performance evaluation of the proposed control method in SimPowerSystems toolbox.

5. CONCLUSIONS

An efficient DC voltage control strategy for the VSC terminal is developed in this paper. A theoretical analysis is carried out by using singular perturbation techniques. In brief, the control structure consists of two subcontrollers. The current subcontroller is used to make $i_{l,dq}$ very quickly enter their respective manifolds $i^*_{l,dq}$ during the initial interval. Assuming that $i_{l,dq}$ remain close to $i^*_{l,dq}$ after a short transient, we can obtain a reduced model by substituting the manifolds $i^*_{l,dq}$ into the DC voltage subsystem where i^*_{ld} is considered as the control input. The DC voltage subcontroller is then designed to make the reduced model converge to u^*_c. It is obvious that the DC voltage subcontroller is actually developed by using the reduced model. This makes the control design process much easier than using the original DC voltage system. We also indicate that, when keeping the control gains of the DC voltage subcontroller unchanged, the performance of the system can be improved by increasing the control gains of the current subsystem.

In order to evaluate the performance of the proposed control method and verify the theoretical analysis, several scenarios are carried out. Simulation results clearly show that this new control scheme can regulate u_c with good performances regardless of the variations in i_c and u^*_c. In addition, u_c can be well approximated by the solution of the reduced model $u_{c,re}$. Moreover, it is clearly clarified that the error between u_c and $u_{c,re}$ can be decreased by giving large control gains to the current subcontroller.

In this paper, the DC voltage subcontroller is developed by using feedback linearization techniques since linear system theory can be easily applied to determine the behavior of the system. In future work, we propose to apply other approaches and then compare the differences between them.

REFERENCES

Blasko, V. and Kaura, V. (1997). A new mathematical model and control of a three-phase AC-DC voltage source converter. *IEEE Transactions on Power Electronics*, 12(1), 116–123.

Chen, Y., Benchaib, A., Damm, G., Lamnabhi-Lagarrigue, F., et al. (2014). A globally stable passiive controller for a VSC-HVDC terminal in a multi-terminal HVDC system. In *Proceedings of the American Control Conference*. Portland, USA.

Chen, Y., Dai, J., Damm, G., Lamnabhi-Lagarrigue, F., et al. (2013). Nonlinear control design for a multi-terminal VSC-HVDC system. In *Proceedings of the European Control Conference*. Zurich, Switzerland.

Flourentzou, N., Agelidis, V.G., and Demetriades, G.D. (2009). VSC-based HVDC power transmission systems: an overview. *IEEE Transactions on Power Electronics*, 24(3), 592–602.

Gomis-Bellmunt, O., Junyent-Ferré, A., Sumper, A., and Bergas-Jané, J. (2011). Control of a wind farm based on synchronous generators with a central HVDC-VSC converter. *IEEE Transactions on Power Systems*, 26(3), 1632–1640.

Liang, J., Gomis-Bellmunt, O., Ekanayake, J., Jenkins, N., and An, W. (2012). A multi-terminal HVDC transmission system for offshore wind farms with induction generators. *International Journal of Electrical Power & Energy Systems*, 43(1), 54–62.

Lindberg, A. and Larsson, T. (1996). PWM and control of three level voltage source back-to-back station.

Zhang, L., Harnefors, L., and Nee, H.P. (2010). Power-synchronization control of grid-connected voltage-source converters. *IEEE Transactions on Power Systems*, 25(2), 809–820.